IEEE Photonics Journal
An IEEE Photonics Society Publication

Analysis on Location Accuracy for the Binocular Stereo Vision System

Volume 10, Number 1, February 2018

Lu Yang
Baoqing Wang
Ronghui Zhang
Haibo Zhou
Rongben Wang

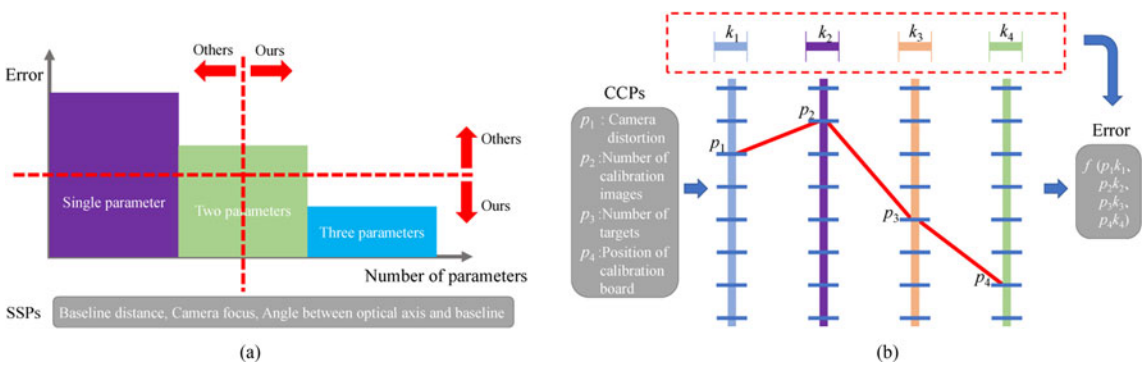

DOI: 10.1109/JPHOT.2017.2784958
1943-0655 © 2017 CCBY

Analysis on Location Accuracy for the Binocular Stereo Vision System

Lu Yang,[1,2] Baoqing Wang,[1,2] Ronghui Zhang,[3] Haibo Zhou,[1,2] and Rongben Wang[4]

[1]Tianjin Key Laboratory for Advanced Mechatronic System Design and Intelligent Control, School of Mechanical Engineering, Tianjin University of Technology, Tianjin 300384, China
[2]National Demonstration Center for Experimental Mechanical and Electrical Engineering Education, Tianjin University of Technology, Tianjin 300384, China
[3]Guangdong Key Laboratory of Intelligent Transportation System, School of Engineering, Sun Yat-sen University, Guangzhou 510275, China
[4]College of Transportation, Jilin University, Changchun 130025, China

DOI:10.1109/JPHOT.2017.2784958

Manuscript received October 28, 2017; revised December 8, 2017; accepted December 13, 2017. Date of publication December 19, 2017; date of current version January 5, 2018. This work was supported in part by the Tianjin Natural Science Foundation of China under Grant 16JCQNJC04100, in part by the National Natural Science Foundation of China under Grants 51275209 and 51775565, in part by the Tianjin Municipal Natural Science Foundation Project supported by the Tianjin Municipal Science and Technology Commission under Grant 17JCZDJC30400, and in part by the Opening Fund of Guangdong Key Laboratory of Intelligent Transportation System under Grant 201701002. Corresponding authors: R. Zhang and H. Zhou (e-mail: zrh1981819@126.com; haibo_zhou@163.com).

Abstract: Binocular stereo vision (BSV) system has been widely used in various fields, such as intelligent manufacture, smart robot, and so on. However, the location accuracy of the current BSV still cannot fully satisfy industry requirements due to lack of a parameters optimization BSV system. In this paper, a high accuracy BSV system is proposed. This is achieved through analyzing the seven parameters of the BSV system, which are classified into two groups: system structure parameters (SSPs) and camera calibration parameters (CCPs). For the SSPs, an improved analysis model is designed to expose the possible errors caused by three parameters. Furthermore, a new correlation model among them is also proposed to analyze the errors caused by their correlation. On the other hand, for the CCPs, the orthogonal experiment model is employed for selecting the optimal combination of the four calibration parameters. Meanwhile, the weight among the four parameters is also analyzed for reducing errors. Finally, the effectiveness of our proposed method is demonstrated by a large number of experiments. It gives a useful reference to the BSV system used in applied optics research and application fields.

Index Terms: Binocular stereo vision system, location accuracy, camera calibration parameter, system structure parameter, applied optics.

1. Introduction

Recently, with the development of industrial intelligence, Binocular Stereo Vision (BSV) system has become more and more important in various application fields [1]–[4]. However, the location accuracy of existing BSV systems cannot fully satisfy industry requirements. This is because most of current BSV systems are built according to engineers' experience, which leads to low location accuracy. Therefore, more and more researchers are focus on designing an optimal BSV system, whose high accuracy can satisfy the harsh requirements [5]–[8]. For obtaining a BSV system with an optimal accuracy, the following two relationships need to be analyzed:

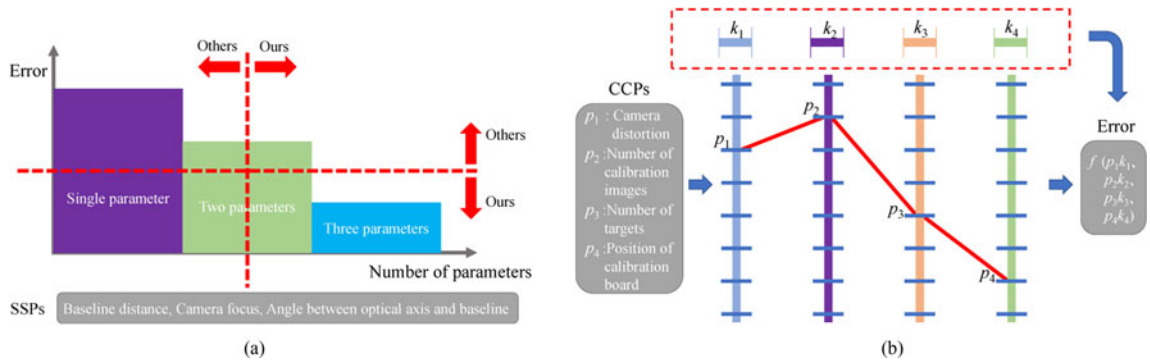

Fig. 1. Our analysis system for SSPs and CCPs. The red dot lines of (a) show that, the error of our method is smaller than others, and the analyzed parameters are more than other methods. Especially, our method is the first work to analyze the correlation of all 3 parameters. In (b), the errors are analyzed by 4 parameters p_i, with the weights k_i ($i = 1, 2, 3, 4$). Here, the 4 parameters are represented using parallel coordinate, as shown in (b). (a) System structure parameters (SSPs). (b) Camera calibration parameters (CCPs).

1) The relationship between each parameter and the possible error.
2) The relationships among all parameters.

In order to fully analyze these two relationships, a well-designed analysis framework is necessary. While existing methods for analysis of accuracy for BSV system are only focus on a few fixed parameters. Even more, no analysis method is designed to expose the above multi-parameters complicated relationships. Cui *et al.* proposed a new bundle adjustment algorithm to improve the accuracy of BSV system [9]. However, this method can only be used for a fixed relative constraint. A perpendicularity compensation method is another recent method for improving the accuracy of BSV system [10]. This method can only be used for some special systems. It cannot be extended to most general systems. All in all, their most serious problem is the scalability.

In this paper, a scalable analysis framework is proposed to guide an optimal parameter selection for users. Under this framework, the accuracy of BSV system is improved through analyzing of all possible factors. These factors are divided into two groups: system structure parameters (SSPs) and camera calibration parameters (CCPs), as shown in Fig. 1. The errors of BSV systems are mainly from the parameters in these two groups. In the system structure group [see Fig. 1(a)], analysis models are designed for the following three parameters: baseline distance, camera focus, and angle between optical axis and baseline. The possible errors caused by them are analyzed in details separately. Meanwhile, the correlation among them is also analyzed for the possible accumulated errors caused by them. This is one of our main contributions. Our method is the first work to analyze all 3 parameters. The errors of our method for single parameter and 2 parameters are also smaller than existing methods. On the other hand, the orthogonal experiment model [11]–[12] is employed for selecting the optimal combination of the 4 calibration parameters. This is another important contribution of our work. As shown in Fig. 1(b), according to the properties of the following 4 parameters, a large number of experiments are carried out: calibration distortion, number of calibration images, number of targets, and position of calibration board. The combination of these 4 parameters and their weights are analyzed by using our proposed method, as shown in Fig. 1(b).

The rest of this paper is organized as follows: Section 2 provides a survey on related works in the fields of accuracy analysis for BSV system. Section 3 explains BSV system as the background knowledge for our proposed approach. Section 4 describes several proposed analysis models for the system structure parameters (SSPs), which is followed by a scheme for experiment analysis of camera calibration parameters (CCPs) in Section 5. Experimental results are also carried out to demonstrate the effectiveness of the proposed analysis framework. Section 6 concludes this paper and refers to possible future extensions.

2. Related Works

Location accuracy analysis of BSV system is a further study in BSV field. Since the BSV system has been put forward, it has been widely used in social productions [13]–[15]. In order to meet the needs of different accuracy demands for BSV system, a vast number of researchers had extended the BSV system to analyze the methods of improving system accuracy. Furthermore, they used analysis tools to analyze the methods of improving system accuracy and express the optimal parameters of research results.

A large number of researches in the field of system accuracy are not comprehensive. They analyzed in the impact of the CCPs of BSV system. Among them, to improve the spatial location precision, many researchers optimized the camera calibration algorithm. Small matrix, derived from Cui *et al*. method, promoted the computational efficiency of camera calibration. To improve the calibration precision, Jia *et al*. added perpendicularity compensation in camera calibration. Fathi *et al*. developed a new calibration method to improve the calibration accuracy. They proved that the method was correct by the 3D points cloud experiments. To an extent, their deep study improved location accuracy of the system. But it did not consider the impact of other important factors in BSV system. So, their researches lacked comprehensive analysis. Liu *et al*., Lu *et al*. and Shih *et al*. made a lot of researches for the SSPs [16]–[18]. Liu *et al*. made a detailed analysis for SSPs of the BSV, which was included the focus, baseline, angle between optical axis and baseline. On the basis of their researches, Lu *et al*. analyzed the impact of CCD pixel discontinuity in BSV system. For the 3D measurement of panoramic camera, Shih *et al*. analyzed the SSPs, and optimized structure algorithms. They analyzed only for the SSPs, and also did not consider the impact of CCPs in BSV system.

At present, most researchers do not consider the reader's information access in the study of BSV system, so that there is no useful reference of the parameter selection. And the experiment method is simple, the analysis is not thorough enough. Liu *et al*. analyzed a lot of the trend of SSPs. But they only gave some changing curve of optical parameters and lacked the comprehensive analysis. Chen *et al*. and Liu *et al*. not only made a comprehensive analysis of the optical parameters in two cameras, but also gave the parametric variation surface and intuitive concise analysis [19]. However, their analysis is not clear and lack the experimental module. Liu *et al*. also made a detailed discussion on the accuracy of the BSV system [20]. Their researches made the theoretical analysis and used charts to show the experimental results. However, the considered factors are lack of comprehensiveness, and the experiment method is single.

In this paper, the factors, affecting the location accuracy for BSV system, includes the SSPs and CCPs. Combining CCPs and SSPs, this paper makes a comprehensive and scientific research, and gives simulation analysis and a lot of experiments to get best optimal parameters.

3. BSV System Model

BSV is an important part of machine vision in industrial intelligence field. Disparity theory is the basic principle of BSV measurement. Firstly, the binocular cameras obtain two images of the measured point from different positions, and then, calculate the position deviation between the corresponding points of the images. Finally, the object 3D information is obtained. This is the process of the BSV imaging measurement.

3.1 Camera Calibration Model

The purpose of camera stereo calibration is to determine the mapping relationship of point between the world coordinate system and the pixel coordinate system [21].

Supposing a point P, whose world coordinate system is (X_W, Y_W, Z_W), camera coordinate system is (X_C, Y_C, Z_C), image coordinate system is (X, Y), and pixel coordinate system is (u, v), as shown

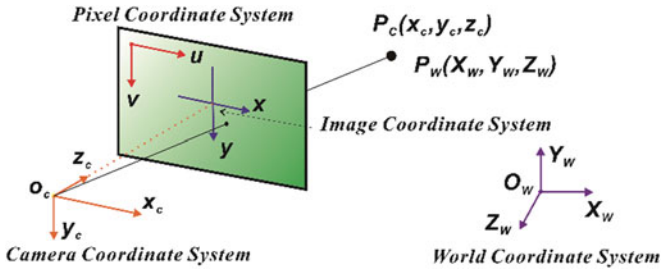

Fig. 2. Coordinate systems.

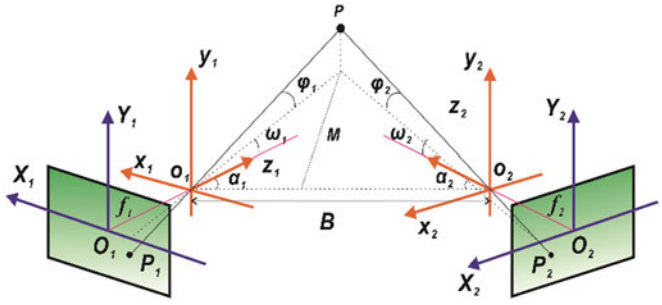

Fig. 3. Principle diagram of accuracy analysis for BSV system.

in Fig. 2. The mapping relationship of them can be represented as followings [22]:

$$s\begin{bmatrix} u \\ v \\ 1 \end{bmatrix} = A\begin{bmatrix} R & t \\ 0^T & 1 \end{bmatrix}\begin{bmatrix} X_W \\ Y_W \\ Z_W \\ 1 \end{bmatrix} \tag{1}$$

$$A = \begin{bmatrix} f_u & \tau & u_o & 0 \\ 0 & f_v & v_o & 0 \\ 0 & 0 & 1 & 0 \end{bmatrix} \tag{2}$$

Matrix A is homogeneous matrix, denotes the camera intrinsic parameters, τ is skew factor, in this paper, we set $\tau = 0$. $\begin{bmatrix} R & t \\ 0^T & 1 \end{bmatrix}$ is camera external parameters, in which R, t, s represent the rotation matrix, translation matrix, and scale factor, respectively. The external parameters can be used to obtain the position relationship among two or more cameras.

3.2 Point Location Model

In order to realize the localization process of a point, a BSV structure model is designed, as shown in Eq. (3). The parameters of the BSV structure model is shown in Fig. 3. The angles between the optical axis and the baseline are α_1 and α_2, the horizontal projection angles are ω_1 and ω_2, the camera focuses are f_1 and f_2, the vertical projection angles are φ_1 and φ_2, the baseline distance is B, and the object distance is M. These parameters are not independent. Their complicated relationship leads that it is difficult to improve the location accuracy of the point.

In Fig. 3, the left camera coordinate system is selected as the world coordinate system. The geometrical relationships between the horizontal projection angle and the vertical projection angle of the camera are shown as follows:

$$\tan\phi_1 = \frac{Y_1 \cdot \cos\omega_1}{f_1}, \quad \tan\phi_2 = \frac{Y_2 \cdot \cos\omega_2}{f_2}, \quad \tan\omega_1 = \frac{X_1}{f_1}, \quad \tan\omega_2 = \frac{X_2}{f_2}$$

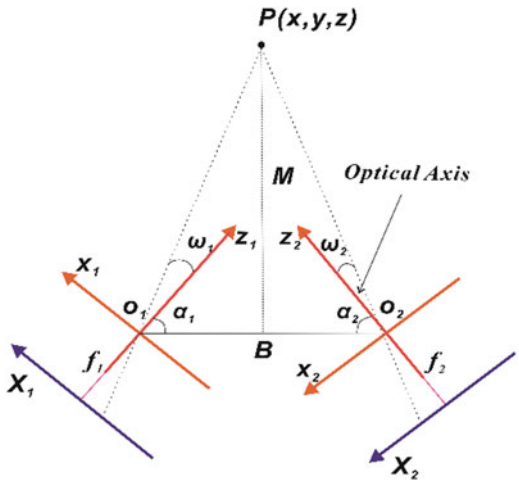

Fig. 4. Simplified model of BSV system.

Let $\theta_1 = \omega_1 + \alpha_1$, $\theta_2 = \omega_2 + \alpha_2$. As shown in Fig. 4, the 3D coordinates of the point P in the world coordinate system can be obtained as:

$$\begin{cases} X_W = \dfrac{B \cdot \cot\theta_1}{\cot\theta_1 + \cot\theta_2} \\ Y_W = \dfrac{Y_1 \cdot \cos\omega_1}{f_1} \cdot \dfrac{M}{\sin\theta_1} = \dfrac{Y_2 \cdot \cos\omega_2}{f_2} \cdot \dfrac{M}{\sin\theta_2} \\ Z_W = \dfrac{B}{\cot\theta_1 + \cot\theta_2} \end{cases} \tag{3}$$

4. Analysis of SSPs

The SSPs of the BSV system include baseline distance B, angle between optical axis and baseline α, camera focus f. $P\,(X_W,\ Y_W,\ Z_W)$ can be expressed as $F\,(B,\ \alpha_1,\ \alpha_2,\ \omega_1,\ \omega_2,\ f_1,\ f_2,\ X_1,\ X_2,\ Y_1,\ Y_2)$. Here, ω is horizontal projection angle, and $(X,\ Y)$ is image coordinate.

According to the synthesis and distribution of error, the total error of system location is represented by the error on X_W, Y_W and Z_W axis. Then, the total error can be obtained as shown in Eq. (4). In order to simplify the research process, the error coefficient δi is not considered. The system error transfer function is as shown in Eq. (5).

$$\gamma = \sqrt{(\Delta X_W)^2 + (\Delta Y_W)^2 + (\Delta Z_W)^2} = \sqrt{\sum_j \sum_i \left(\frac{\partial F}{\partial i} \bullet \delta_i\right)} \tag{4}$$

$$\gamma_i = \sqrt{\sum_j \left(\frac{\partial F_j}{\partial i}\right)^2} \tag{5}$$

Where, γ is total error, γ_i is error caused by parameter i, i is one of the parameters including B, α_1, α_2, ω_1, ω_2, f_1, f_2, X_1, X_2, Y_1, *and* Y_2, j represents direction of X_W, Y_W or Z_W, δi is error coefficient.

4.1 Baseline Distance

The baseline distance B between the two cameras is an important parameter in the binocular stereo vision system. A small change of B will lead to a complicated transformation of the binocular system

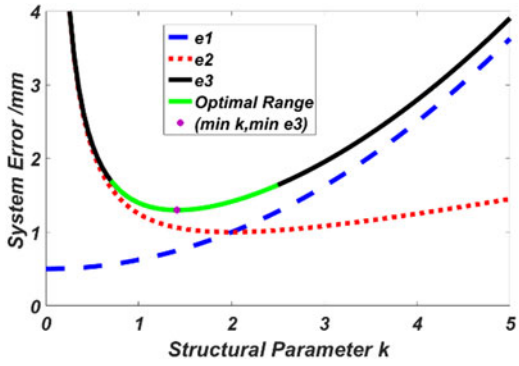

Fig. 5. Relationship curve between parameter k and system error.

structure and the location accuracy. In this section, the relationship between the baseline distance B and the error will be analyzed in 2 steps: obtain the relationship formula and analyze it.

Firstly, obtain the relationship formula. Supposing that the point P is located at the intersection of the two cameras axis. Let $\alpha_1 = \alpha_2 = \alpha$, $\omega_1 = \omega_2 = 0^\circ$, $\varphi_1 = \varphi_2 = 0^\circ$, $f_1 = f_2 = 0$. Using Eq. (3), the world coordinate (X_W, Y_W, Z_W) can be obtained as Eqs. (6) and (7). Note that, $Y_W = 0$. This means that the baseline distance B produces errors only in the horizontal plane (X_W and Z_W directions).

$$\begin{cases} \dfrac{\partial X_W}{\partial X_1} = -\dfrac{M^2}{f \cdot B} \bullet \dfrac{\cot\alpha}{\sin^2\alpha} \\ \dfrac{\partial X_W}{\partial X_2} = -\dfrac{M^2}{f \cdot B} \bullet \dfrac{\cot\alpha}{\sin^2\alpha} \end{cases} \tag{6}$$

$$\begin{cases} \dfrac{\partial Z_W}{\partial X_1} = \dfrac{M^2}{f \cdot B} \bullet \dfrac{1}{\sin^2\alpha} \\ \dfrac{\partial Z_W}{\partial X_2} = \dfrac{M^2}{f \cdot B} \bullet \dfrac{1}{\sin^2\alpha} \end{cases} \tag{7}$$

Let $k = B/M$, $e_1 = \frac{1}{k} \cdot \frac{\cot\alpha}{\sin^2\alpha}$, $e_2 = \frac{1}{k} \cdot \frac{1}{\sin^2\alpha}$, the measurement error of P in the X_W direction and Z_W direction are:

$$\gamma_{B\Delta X} = \sqrt{\left(\frac{\partial X_W}{\partial X_1}\right)^2 + \left(\frac{\partial X_W}{\partial X_2}\right)^2} = \frac{\sqrt{2} \cdot M}{f} e_1 \tag{8}$$

$$\gamma_{B\Delta Z} = \sqrt{\left(\frac{\partial Z_W}{\partial X_1}\right)^2 + \left(\frac{\partial Z_W}{\partial X_2}\right)^2} = \frac{\sqrt{2} \cdot M}{f} e_2 \tag{9}$$

Therefore, the total measurement error caused by baseline distance B can be obtained using Eqs. (5), (8), and (9):

$$\gamma_B = \sqrt{\Delta X^2 + \Delta Z^2} = \frac{\sqrt{2} \cdot M}{f} e_3 \tag{10}$$

Secondly, analyze the obtained above relationship formula. From the above analysis, k can be used to instead of B, to analyze the relationship between the error and the baseline distance. This is because $k = B/M$, and M is a fixed parameter. However, from Eq. (10), it is difficult to explain the relationship due to the complicated Trigonometric functions. Therefore, we use Taylor's formula to replace α using k, as $e_1 = \frac{1}{2} + \frac{k^2}{8}$, $e_2 = \frac{1}{k} + \frac{k}{4}$. Associated with Eqs. (8), (9), and (10), the final relationship between the errors and the baseline distance can be obtained as Fig. 5.

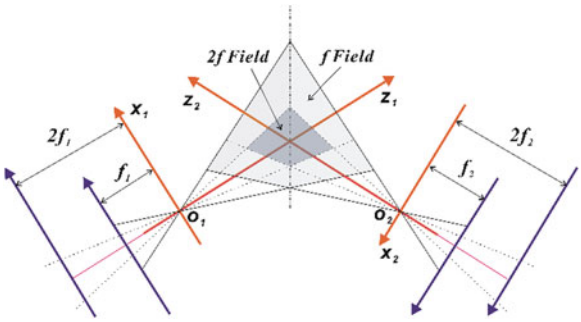

Fig. 6. Change of focal length for BSV system.

In Fig. 5, e_3 combines three directions error of P, which include X axis, Y axis (equal to 0), and Z axis. The trend of e_3 curve is going down first and then going up. When $k = 1.41$, the minimum synthetic error (e_3) can be obtained. Due to $k = B/M$, we could get the following conclusions:

When $M \leq B \leq 2\,\mathrm{M}$, the smallest location error can be obtained. When $0.5\,\mathrm{M} < B < 0.7\,\mathrm{M}$, the location error is too large to be accepted. Note that the data of K should be adjusted according to the specific conditions, and make it close to 1.41.

4.2 Camera Focus

The focal length of the camera is approximately equal to the distance between the camera lens center and the CCD imaging sensor. In this section, the relationship between the focal length and the error of BSV system will be analyzed. Fig. 6 shows that when other parameters are constant in BSV system, with the camera focal length increasing, the FOV becomes narrow. The object should be placed in the common area of two different focal lengths when collecting images.

According to Eqs. (3) and (5), the error transfer functions of two camera focus f_1 and f_2 in BSV system can be obtained.

$$\gamma_{f_1} = \sqrt{\frac{B^2\tan^2\omega_1(\cot^2\theta_1+1)^2}{{f_1}^2(\tan^2\omega_1+1)^2(\cot\theta_1+\cot\theta_2)^4}+\frac{M^2\tan^2\phi_1(\cos(2\theta_1-2\omega_1)-1)}{2{f_1}^2\sin^4\theta_1\cos^4\omega_1(\tan^2\omega_1+1)^3}+\frac{B^2\cot^2\theta_2\tan^2\omega_1(\cot^2\theta_1+1)^2}{{f_1}^2(\tan^2\omega_1+1)^2(\cot\theta_1+\cot\theta_2)^4}} \tag{11}$$

$$\gamma_{f_2} = \sqrt{\frac{B^2\tan^2\omega_2(\cot^2\theta_2+1)^2}{{f_2}^2(\tan^2\omega_2+1)^2(\cot\theta_1+\cot\theta_2)^4}+\frac{M^2\tan^2\phi_2(\cos(2\theta_2-2\omega_2)-1)}{2{f_2}^2\sin^4\theta_2\cos^4\omega_2(\tan^2\omega_2+1)^3}+\frac{B^2\cot^2\theta_1\tan^2\omega_2(\cot^2\theta_2+1)^2}{{f_2}^2(\tan^2\omega_2+1)^2(\cot\theta_1+\cot\theta_2)^4}} \tag{12}$$

Using Eqs. (11) and (12), different focal length of the system error distribution curves can be obtained. As shown in Fig. 7, with the camera focal length increasing and FOV decreasing, the system error is decreasing.

4.3 Angle Between Optical Axis and Baseline

The angle α, between the optical axis and the baseline, is also a key factor that affects the location accuracy. According to Eqs. (3) and (5), the error transfer function about α_1 and α_2 can be obtained as followings:

$$\gamma_{\alpha_1} = \sqrt{\frac{B^2(\cot^2\theta_1+1)^2}{(\cot\theta_1+\cot\theta_2)^4}+\frac{B^2\cot^2\theta_2(\cot^2\theta_1+1)^2}{(\cot\theta_1+\cot\theta_2)^4}+\frac{B^2\cot^2\theta_1\tan^2\phi_1}{\sin^4\theta_1(\cot\theta_1+\cot\theta_2)^2}} \tag{13}$$

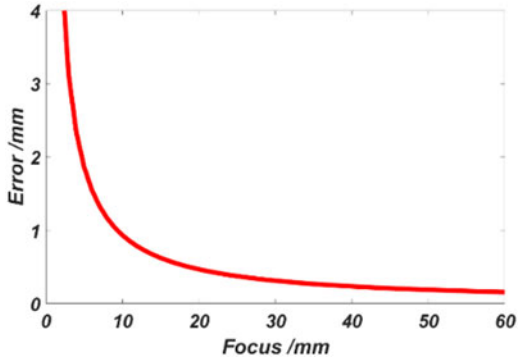

Fig. 7. Impact of focal length on system error.

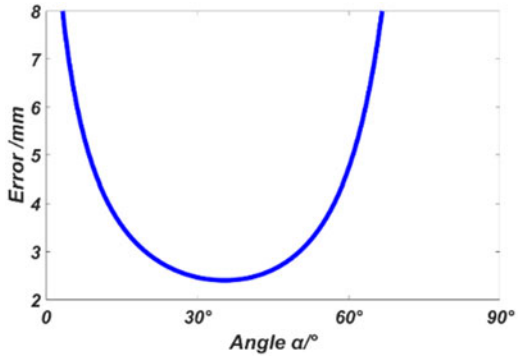

Fig. 8. Impact of the angle between the optical axis and the baseline on system error.

$$\gamma_{\alpha_2} = \sqrt{\frac{B^2(\cot^2\theta_2+1)^2}{(\cot\theta_1+\cot\theta_2)^4} + \frac{B^2\cot^2\theta_1(\cot^2\theta_2+1)^2}{(\cot\theta_1+\cot\theta_2)^4} + \frac{B^2\cot^2\theta_2\tan^2\phi_2}{\sin^4\theta_2(\cot\theta_1+\cot\theta_2)^2}} \tag{14}$$

Using Eqs. (13) and (14), the error curve of α_1 and α_2 can be obtained, as shown in Fig. 8.

From Fig. 8, we can know that the relationship between the angle and the error is a parabola. The critical point is nearby 36°. In our method, we recommend that the range of angle α should be from 30° to 45°. This is because the change is slow in the troughs of the parabola.

4.4 Comprehensive Analysis

Three structural parameters (B, f, α) have been separately analyzed above. However, the single variable range cannot analyze the complex constraint relationship among the three parameters. This section makes an analysis of the combination of all three parameters. This is one of our main contributions. Using Eqs. (10), (11), and (13), the comprehensive transfer function can be obtained as:

$$\begin{cases} \gamma_\alpha = \sqrt{\frac{B^2(\cot^2\theta+1)^2}{(2\cot\theta)^4} + \frac{B^2\cot^2\theta(\cot^2\theta+1)^2}{(2\cot\theta)^4} + \frac{B^2\cot^2\theta\tan^2\phi}{\sin^4\theta(2\cot\theta)^2}} \\ \gamma_f = \sqrt{\frac{B^2\tan^2\omega(\cot^2\theta+1)^2}{f^2(\tan^2\omega+1)^2(2\cot\theta)^4} + \frac{M^2\tan^2\phi(\cos(2\theta-2\omega)-1)}{2f^2\sin^4\theta\cos^4\omega(\tan^2\omega+1)^3} + \frac{B^2\cot^2\theta\tan^2\omega(\cot^2\theta+1)^2}{f^2(\tan^2\omega+1)^2(2\cot\theta)^4}} \\ \gamma_B = \sqrt{\frac{\cos(2\theta)-1}{\cos(4\theta)-1}} \\ B = nL\,(n=1,2,3,4,5\ldots) \end{cases} \tag{15}$$

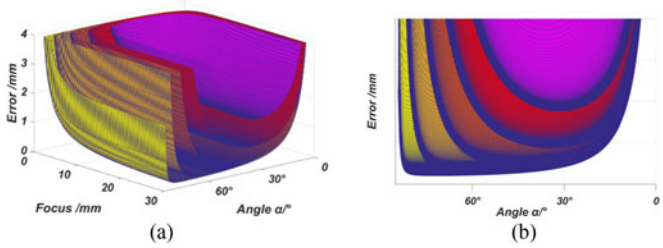

Fig. 9. Comprehensive analysis of the three parameters.

Fig. 9 is the result of the comprehensive analysis using Eq. (15). 5 different baseline distances are analyzed, represented by different surface with different colors in Fig. 9. Each surface shows the relationship between the focus f, the angle α, and the system error. From the inside surface (purple) to the outside surface (yellow), the value of B is increasing. It can be seen that with B increasing, the surface moves down and expands. The system error is reduced. With the focus increasing, the surface drops. The system error is gradually reduced. From the right side to see, the angle α is U-shaped changes, the detail is shown in Fig. 9(b). The critical point with smallest error can be obtained. Using the above comprehensive analysis, a high-precision location can be obtained.

5. Analysis of CCPs

Camera calibration parameters (CCPs) affect the location accuracy of BSV system. In this section, we will analyze the impact of 4 CCPs, including camera distortion (see Section 5.1), number of calibration images (see Section 5.2), number of targets (see Section 5.3), and position of calibration board (see Section 5.4). The controlled variable approach will be used for analysis of the error from one of the four CCPs. Furthermore, the orthogonal experiment method will be employed to analyze the error caused by the combination of 4 CCPs (see Section 5.5).

Two Manta G-201C camera of IMAVISION are used to carry out the location experiment. The calibration distance is about 2.5 m, the angle between tilted board and camera plane should be less than 45°, and the checkerboard is placed on the surface of the calibration board. The actual size of each checkerboard is 30 $\times$ 30 mm, the number of used images is 13. The light source is natural light. In the progress of calibration, the SSPs are set to the best values based on the analysis of Section 4. The Precision will be analyzed using Eq. (5). γ means the difference between the locating coordinate and the actual coordinate.

5.1 Camera Distortion

In practical applications, the lens manufacturing process is not perfect and the lens exist errors in the assembly process. The lens error would lead to the small amount of image distortion.

The linear camera model is an ideal camera model, in which the distortion caused by the manufacture and assembly of camera lens is ignored. The linear model is widely used in existing method, because it is very simple. However, the linear model will cause large error. In our proposed method, nonlinear model will be used to analyze and correct the error caused by the distortion.

Nonlinear distortion is generally regarded as geometric distortion. It makes an offset between the point of the captured image and the position of its ideal point. Correcting distortion is to remove the offset as much as possible. Fig. 10 is a schematic diagram of lens distortion.

$$\begin{cases} x' = x + \delta_x(x, y) \\ y' = y + \delta_y(x, y) \end{cases} \tag{16}$$

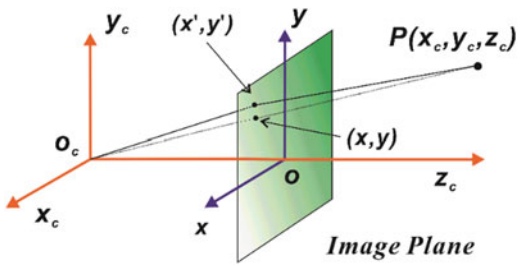

Fig. 10. Schematic diagram of nonlinear model.

TABLE 1
Internal Parameters

Internal parameters	f_x	f_y	u_0	v_0	α
Left camera	2729.02	2731.02	795.92	658.35	−0.48
Right camera	2738.21	2740.26	800.87	604.33	1.54

In Eq. (16), $(x',\ y')$ is the coordinate of the actual projection P in the image coordinate system. $(x,\ y)$ is the coordinate of the projection point. δ_x and δ_y are the offsets produced by distortion along the X and Y directions. The distortion includes radial distortion and tangential distortion. The radial distortion is mainly caused by radial curvature of optical lens [23]. This distortion causes the image point to move inward or outward along the radial direction. The farther away from the center, the greater is the deformation. δ_{xr} and δ_{yr} are radial distortion deviations along the X and Y directions, respectively. The tangential distortion is caused by the defect of the lens manufacturer. It makes the lens itself not parallel to the image plane. δ_{xt} and δ_{yt} are tangential distortion deviations along the X and Y directions, respectively.

$$\begin{cases} r^2 = x^2 + y^2 \\ \delta_{xr} = x\left(k_1 r^2 + k_2 r^4 + k_3 r^6\right) \\ \delta_{yr} = y\left(k_1 r^2 + k_2 r^4 + k_3 r^6\right) \\ \delta_{xt} = p_1\left(r^2 + 2x^2\right) + 2p_2 xy \\ \delta_{yt} = p_2\left(r^2 + 2y^2\right) + 2p_1 xy \end{cases} \tag{17}$$

Where, $k_1,\ k_2,\ k_3$ are radial distortion factors. The $p_1,\ p_2$ are tangential distortion coefficients. The radical distortion and the tangential distortion in Eq. (17) can be synthesized as the final distortion as Eq. (18) [24].

$$\begin{cases} \delta_x = x\left(k_1 r^2 + k_2 r^4 + k_3 r^6\right) + p_1\left(r^2 + 2x^2\right) + 2p_2 xy \\ \delta_y = y\left(k_1 r^2 + k_2 r^4 + k_3 r^6\right) + p_2\left(r^2 + 2y^2\right) + 2p_1 xy \end{cases} \tag{18}$$

Finally, the effectiveness of our nonlinear method will be demonstrated through comparing the error with the linear method. The calibration parameters in Tables 1–3 are used to locate the spatial positions of the experimental balls (3D reconstruction). Here, the parameters in Tables 1 and 2 are the common parameters of linear and nonlinear models, while Table 3 is the parameters for nonlinear model. Table 4 is the results from linear model and nonlinear model. The error using nonlinear method is smaller than the linear method, thanks to the distortion correction process of nonlinear model.

TABLE 2
Camera Distortion Parameters

Distortion factor	k_1	k_2	p_1	p_2
Left camera	−0.078	0.207	0.003	0.002
Right camera	−0.121	0.763	9.108	−0.003

TABLE 3
External Parameters

Symbol	External parameter
R	$\begin{bmatrix} 0.9998 & -0.0015 & 0.0198 \\ 0.0018 & 0.9999 & -0.0145 \\ -0.0198 & 0.0146 & 0.9997 \end{bmatrix}$
t	$[-393.1541 \quad 0.1754 \quad 1.0065]$

TABLE 4
Comparison Analysis for Camera Distortion

Model types	Small ball's space measurement coordinate (mm)	Small ball binocular coordinate (mm)	γ
Linear model (undistorted)	(0, 150, –20)	(0.2, 150.3, –19.9)	0.374
Nonlinear model (with distortion)	(0, 150, –2)	(0.1, 150.3, –20.1)	0.332

5.2 Number of Calibration Images

In this section, we will analyze the relationship between the location error and the number of calibration images. In our experiment, 19 images are collected, and then the n images ($n = 3, 5, 7 \ldots, 19$) are selected for calibration. It can be seen from Fig. 11 that the calibration error is the largest when the number of calibration images is 3. With the number of calibration images increasing gradually, the calibration error is decreasing. When the number of calibration images is 13, it can be seen that the location error tends to be stable. Therefore, when the camera is calibrated, the image number of the calibration board should be more than 13.

5.3 Number of Targets

The target number of the calibration board cannot be ignored in camera calibration. It also affects the camera calibration accuracy. In essence, camera calibration is a data fitting process. The data fit is closely related to the spatial distribution of sample data. The number of target arrays affects

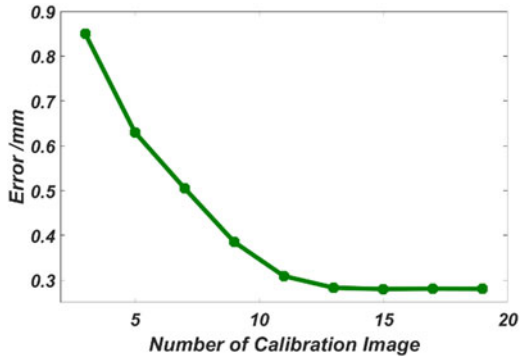

Fig. 11. Impact of the number of calibrated images on the calibration accuracy.

Fig. 12. Calibration boards for different target numbers. (a) 5 × 7, (b) 6 × 9, (c) 7 × 9, (d) 8 × 11, and (e) 9 × 11.

TABLE 5
Comparison Analysis for Number of Targets

Board size	Ball's measurement coordinate (mm)	Ball's calculation coordinate (mm)	γ
5 × 7 board	(0, 161, –20)	(0.3, 160.9, –19.8)	0.374
7 × 9 board	(0, 161, –20)	(0.2, 160.8, –19.9)	0.300
9 × 11 board	(0, 161, –20)	(–0.2, 161, –20.2)	0.283

the number of fitting points in the calculation. That is to say, the more the number of targets, the more the sample data, the closer the fitting result to the real value. Fig. 12 shows calibration boards for different target numbers. In this experiment, five types of boards are compared. The number of corners, identified in five boards, is 24, 40, 48, 70 and 80 respectively.

According to experimental results in Table 5, it can be seen clearly that when using 9 × 11 [see Fig. 12(e)] calibration board for experiments, the accuracy obtained by ball location is the highest. It can be concluded that, the more the number of targets, the higher is the accuracy of the CCPs, the smaller is the error of small ball location.

5.4 Position of Calibration Board

When the camera is calibrated, the position of the calibration board must be placed in the FOV of camera. So that the board image can be clearly identified. The FOV of camera is a space area (the gray area of Fig. 6). When the images are collected, the calibration board can be placed in arbitrary position of the FOV. The most important is the location of the board in the image and the size of the image area. As a valid image, the board should fill at least 30% of the captured images.

TABLE 6
Camera Rotation Parameters for Different Positions of Calibration Board

Position	R_{11}	R_{12}	R_{13}	R_{21}	R_{22}	R_{23}	R_{31}	R_{32}	R_{33}
Lower left	0.992	−0.004	−0.129	0.003	1.000	−0.004	0.129	0.004	0.992
Upper left	0.992	−0.008	−0.124	0.007	0.999	−0.010	0.124	0.009	0.992
Lower right	0.992	0.002	−0.128	−0.004	0.999	−0.017	0.128	0.017	0.992
Upper right	0.992	0.000	−0.127	−0.002	1.000	−0.009	0.127	0.009	0.992
Random	0.991	−0.001	−0.134	0.002	1.000	0.004	0.134	−0.004	0.991

TABLE 7
Camera Translation Parameters for Different Positions of Calibration Board

Position	t_1	t_2	t_3
Lower left	−381.0702	−0.6891	25.8675
Upper left	−379.6840	1.9480	30.3007
Lower right	−380.1994	−2.7178	36.2198
Upper right	−384.0236	1.2791	28.2429
Random	−380.9000	−0.5681	33.3083

TABLE 8
Comparison Analysis for Different Positions of Calibration Board

Position	Ball's measurement coordinate (mm)	Ball's calculation coordinate (mm)	γ
Lower left	(0, 160, −20)	(0.2, 159.6, −19.9)	0.458
Upper left	(0, 160, −20)	(0.1, 159.6, −20.1)	0.424
Lower right	(0, 160, −20)	(−0.3, 160.3, −19.9)	0.436
Upper right	(0, 160, −20)	(−0.2, 160.4, −19.9)	0.458
Random	(0, 160, −20)	(−0.1, 159.8, −20.2)	0.300

In this experiment, the calibration board is set at 5 special areas of the FOV: lower left, upper left, lower right, upper right, center and random. At each area, 13 images will be captured by each camera. Tables 6 and 7 show the obtained 5 groups of camera parameters. In order to test the effect of camera calibration results on the location accuracy, 5 groups of small ball space location experiments are carried out. The results are shown in Table 8.

In Table 8, it is clear that the location error in the "Random" area is the smallest. This is because the 13 images in the "Random" area are evenly distributed in the whole FOV. On the other hand, the 13 images of "Lower left" area are only from the "Lower left" area of the FOV. The same are the remained 3 areas ("Upper left, Lower right, and Upper right").

TABLE 9
The Orthogonal Table of $L_{25}(5^3)$ and Data Processing

Trial no.	Factors: Number of calibration images A[a]	Factors: Number of targets B[b]	Factors: Position of calibration boards C[c]	Experiment result Y_{ji}[d]
1	1	1	1	1.168
2	1	2	2	0.955
3	1	3	3	0.835
4	1	4	4	0.797
5	1	5	5	0.692
6	2	1	2	0.850
7	2	2	3	0.718
8	2	3	4	0.692
9	2	4	5	0.559
10	2	5	1	0.541
11	3	1	3	0.569
12	3	2	4	0.531
13	3	3	5	0.484
14	3	4	1	0.472
15	3	5	2	0.387
16	4	1	4	0.357
17	4	2	5	0.346
18	4	3	1	0.331
19	4	4	2	0.327
20	4	5	3	0.326
21	5	1	5	0.331
22	5	2	1	0.329
23	5	3	2	0.322
24	5	4	3	0.315
25	5	5	4	0.328
$\bar{K}_1$	0.889[e]	0.655	0.568	
$\bar{K}_2$	0.672	0.576	0.568	
$\bar{K}_3$	0.489	0.533	0.553	$T = \sum_{j=A,B,C} \sum_{i=1}^{5} Y_{ji}$
$\bar{K}_4$	0.337	0.494	0.541	
$\bar{K}_5$	0.325	0.455	0.482	
Range[f]	0.564	0.200	0.086	

[a] 1–5 in the column of Number of calibration images ($A1 - A5$) represent 7, 9, 11, 13 and 15 images respectively.
[b] 1–5 in the column of Number of targets ($B1 - B5$) represent 5×7, 6×9, 7×9, 8×11 and 9×11 board respectively.
[c] 1–5 in the column of Position of calibration boards ($C1 - C5$) represent upper left, lower left, upper right, lower right and random position respectively.
[d] $Y_{ji} = \gamma$, this is shown in Eq. (4). ($i = 1, 2, 3, 4, 5$; $j = A, B, C$).
[e] $\bar{K}_{ji} = \frac{K_{ji}}{5} = \frac{\sum_{i=1}^{5} Y_{ji}}{5}$, $\bar{K}_{A1} = \frac{K_{A1}}{5} = \frac{\sum_{i=1}^{5} Y_{A1}}{5} = \frac{1.168+0.955+0.835+0.797+0.692}{5} \approx 0.889$. ($i = 1, 2, 3, 4, 5$; $j = A, B, C$).
[f] $R_j(Range) = \max(\bar{K}_{ji}) - \min(\bar{K}_{ji})$. ($i = 1, 2, 3, 4, 5$; $j = A, B, C$).

5.5 Comprehensive Analysis

The above four sections make a theoretical analysis of CCPs in details, and quantify the influence of various parameters on the location accuracy by experimental analysis. However, we do not know the correlation among the four and significance of impact on accuracy. Therefore, orthogonal experimental design is used to analyze the comprehensive impact on accuracy of CCPs [25]–[26]. Due to the smaller error with distortion nonlinear model [27], we made 3 factors and 5 levels of orthogonal analysis for the other 3 factors in CCPs, a total of 25 experiments. Table structure and experimental results are shown in Table 9. Finally, the range analysis method is used to analyze the experimental data, and the significance of the 3 parameters on the location accuracy is obtained.

There are two important parameters in a range analysis: K_{ji} and R_j (*Range*). K_{ji} is defined as the sum of the evaluation indices of all levels ($i = 1, 2, 3, 4, 5$) in each factor ($j = A, B, C$), and $\bar{K}_{ji}$ (value of K_{ji}) is used to determine the optimal level and the optimal combination of factors. The optimal level for each factor could be obtained when $\bar{K}_{ji}$ is the minimum. R_j is defined as the range between the maximum and minimum value of $\bar{K}_{ji}$ and is used for evaluating the importance of the factors, i.e., the minimum R_j means a greater importance of the factor. Among them, in the A (number of calibration images) column, $\Delta_4 = \bar{K}_4 - \bar{K}_5$ is less than $\Delta_3 = \bar{K}_3 - \bar{K}_4$, $\Delta_2 = \bar{K}_2 - \bar{K}_3$ and $\Delta_1 = \bar{K}_1 - \bar{K}_2$, and the conclusion is consistent with the Section 4.2 analysis. When the number of images is 13, the optimal parameters exist. Because $R_A > R_B > R_C$ in the range analysis, the number of calibration images has much significant influence on the spatial location accuracy, and the position of calibration boards has less impact on the spatial location accuracy.

6. Conclusions

In this paper, we analyze the impact of various parameters in location accuracy in details. This is achieved through analyzing all the possible factors that can cause errors in the BSV system. We divide these factors into two groups: system structure parameters (SSPs) and camera calibration parameters (CCPs).

For the SSPs, 3 parameters (baseline distance, focal length, angle) are analyzed one by one firstly, followed by the comprehensive analysis of the error caused by the combination of these 3 parameters. Our method is the first work to analyze the intersect affection of these 3 parameters on the location accuracy of the BSV system.

For the CCPs, 4 parameters (camera distortion, number of calibration images, number of targets, and position of calibration board) are separately analyzed using the controlled variable approach. Furthermore, the orthogonal experiment method is employed to analyze the affection of the combination the 4 parameters on the location accuracy.

Nowadays, as an important application field, Binocular Stereo Vision (BSV) system has been widely used in intelligent transportation system, while its accuracy still cannot satisfy industrial requirements [28]–[30]. One of possible future work, is to perform the parametric simulation for the analysis of CCPs. Meanwhile, a more useful reference of parameters selection will be given for the BSV system used in other various researches and application fields [31]–[38].

Acknowledgment

The authors declare that there is no conflict of interests regarding the publication of this article.

References

[1] H. Fathi and I. Brilakis, "A multi-step explicit stereo camera calibration approach to improve Euclidean accuracy of large-scale 3D reconstruction," *J. Comput. Civil Eng.*, vol. 30, no. 1, 2016, Art. no. 04014120.
[2] X. Z. Chen and S. B. Chen, "The autonomous detection and guiding of start welding position for arc welding robot," *Ind. Robot*, vol. 37, no. 1, pp. 70–78, 2010.
[3] H. Jiang, T. Zhang, J. P. Wachs, and B. S. Duerstock, "Enhanced control of a wheelchair-mounted robotic manipulator using 3-D vision and multimodal interaction," *Comput. Vis. Image Understanding*, vol. 149, pp. 21–31, Apr. 2016.

[4] R. Anchini, G. Di Leo, C. Liguori, and A. Paolillo, "Metrological characterization of a vision-based measurement system for the online inspection of automotive rubber profile," *IEEE Trans. Instrum. Meas.*, vol. 58, no. 1, pp. 4–13, Jan. 2009.
[5] W. Sankowski, M. Włodarczyk, D. Kacperski, and K. Grabowski, "Estimation of measurement uncertainty in stereo vision system," *Image Vis. Comput.*, vol. 61, pp. 70–81, 2017.
[6] F. Fooladgar, S. Samavi, S. M. R. Soroushmehr, and S. Shirani, "Geometrical analysis of localization error in stereo vision systems," *Sensors*, vol. 13, no. 11, pp. 4236–4246, 2013.
[7] K. Schreve, "How accurate can a stereovision measurement be?" in *Proc. 2014 15th Int. Workshop Res. Educ. Mechatronics*, 2014, pp. 1–7.
[8] G. Di Leo and A. Paolillo, "Uncertainty evaluation of camera model parameters," in *Proc. 2011 IEEE Conf. Instrum. Meas. Technol.*, 2011, pp. 1–6.
[9] J. Cui, J. Huo, and M. Yang, "Novel method of calibration with restrictive constraints for stereo-vision system," *J. Mod. Opt.*, vol. 63, no. 9, pp. 835–846, 2016.
[10] Z. Jia *et al.*, "Improved camera calibration method based on perpendicularity compensation for binocular stereo vision measurement system," *Opt. Exp.*, vol. 23, no. 12, pp. 15205–15223, 2015.
[11] P. J. Ross, *Taguchi Techniques for Quality Engineering: Loss Function, Orthogonal Experiments, Parameter and Tolerance Design*. New York, NY, USA: McGraw-Hill, 1996.
[12] D. K. J. Lin, "Statistics for experimenters: Design, innovation, and discovery, second edition," *J. Qual. Technol., Quart. J. Methods Appl. Relat. Topics*, vol. 38, pp. 78–80, 2006.
[13] I. T. Comlekciler, S. Gunes, and C. Irgin, "Artificial 3-D contactless measurement in orthognathic surgery with binocular stereo vision," *Appl. Soft Comput.*, vol. 41, pp. 505–514, 2016.
[14] C. Wang, X. Zou, Y. Tang, L. Luo, and W. Feng, "Localisation of litchi in an unstructured environment using binocular stereo vision," *Biosyst. Eng.*, vol. 145, pp. 39–51, 2016.
[15] H. Li, Y. Chen, T. Chang, X. Wu, Y. Ou, and Y. Xu, "Binocular vision positioning for robot grasping," in *Proc. IEEE Int. Conf. Robot. Biomimetics*, 2011, pp. 1522–1527.
[16] Q. Liu, X. Qin, S. Yin, and F. He, "Structural parameter design and accuracy analysis of binocular vision measuring system," *China Mech. Eng.*, vol. 19, no. 22, pp. 2728–2732, 2008.
[17] B. Lu, Y. Liu, and L. Su, "Error analysis of binocular stereo vision system applied in small scale measurement," *Acta Photon. Sin.*, vol. 44, no. 10, pp. 1011001-1–1011001-6, 2015.
[18] S. E. Shih and W. H. Tsai, "Optimal design and placement of omni-cameras in binocular vision systems for accurate 3-D data measurement," *IEEE Trans. Circuits Syst. Video Technol.*, vol. 23, no. 11, pp. 1911–1926, Nov. 2013.
[19] Z. Chen, W. Wang, F. Wang, and H. Wang, "Precision analysis and selection design of parallel binocular stereo vision sensor," in *Proc. IEEE Int. Conf. Comput. Sci. Netw. Technol.*, 2013, pp. 1550–1553.
[20] J. Liu, Y. Zhang, and Z. Li, "Selection of cameras setup geometry parameters in binocular stereovision," in *Proc. IEEE Conf. Robot. Autom. Mechatronics*, 2006, pp. 1–6.
[21] Z. Y. Zhang, "A flexible new technique for camera calibration," *IEEE Trans. Pattern Anal. Mach. Intell.*, vol. 22, no. 11, pp. 1330–1334, Nov. 2000.
[22] G. Y. Xu, L. P. Chen, and F. Gao, "Study on binocular stereo camera calibration method," in *Proc. IEEE Int. Conf. Image Anal. Signal Process.*, 2011, pp. 133–137.
[23] X. Li, J. Yao, and J. Zhang, "Comparison and selection of camera models with lens distortion," *J. Comput.-Aided Des. Comput. Graph.*, vol. 27, no. 5, pp. 824–831, 2015.
[24] *OpenCV Reference Manual*, Release 3.0.0-dev, 2015. [Online]. Available: https://docs.opencv.org/3.0.0/
[25] P. Duan, Y. Wang, Y. Yang, and L. Dai, "Optimization of adiponitrile hydrolysis in subcritical water using an orthogonal array design," in *J. Solut. Chem.*, vol. 38, no. 2, pp. 241–258, 2009.
[26] C. Cui, S. Feng, Y. Li, and S. Wang, "Orthogonal analysis for perovskite structure microwave dielectric ceramic thin films fabricated by the RF magnetron-sputtering method," *J. Mater. Sci. Mater. Electron.*, vol. 21, no. 4, pp. 349–354, 2010.
[27] Y. Xu, Y. Zhao, F. Wu, and K. Yang, "Error analysis of calibration parameters estimation for binocular stereo vision system," in *Proc. IEEE Int. Conf. Imag. Syst. Techn.*, 2014, pp. 317–320.
[28] R. H. Zhang, Z. C. He, H. W. Wang, Y. Feng, and K. N. Li, "Study on self-tuning tyre friction control for developing main-servo loop integrated chassis control system," *IEEE Access*, vol. 5, no. 99, pp. 6649–6660, 2017.
[29] R. H. Zhang, J. P. Wu, L. Huang, and F. You, "Study of bicycle movements in conflicts at mixed traffic unsignalized intersections," *IEEE Access*, vol. 5, no. 99, pp. 10108–10117, May 2017.
[30] R. H. Zhang, F. You, F. Chen, and W. Q. He, "Vehicle detection method for intelligent vehicle at night time based on video and laser information," *Int. J. Pattern Recognit. Artif. Intell.*, vol. 32, no. 4, pp. 1850009-1–1850009-20, 2018.
[31] C. Bi, Y. Yuan, R. Zhang, Y. Xiang, Y. Wang, and J. Zhang, "A dynamic mode decomposition based edge detection method for art images," *IEEE Photon. J.*, vol. 9, no. 6, pp. 7803813-1–7803813-13, Dec. 2017.
[32] M. Sun, W. Chen, T. Liu, and L. Li, "Image retrieval in spatial and temporal domains with a quadrant detector," *IEEE Photon. J.*, vol. 9, no. 5, Oct. 2017, Art. no. 3901206.
[33] W. Huang and Z. Xu, "Characteristics and performance of image sensor communication," *IEEE Photon. J.*, vol. 9, no. 2, pp. 1–19, Apr. 2017.
[34] Y. Zhao, Q. Chen, X. Sui, and H. Gao, "Super resolution imaging based on a dynamic single pixel camera," *IEEE Photon. J.*, vol. 9, no. 2, pp. 1–11, Apr. 2017.
[35] H. Huang, A. Yang, L. Feng, G. Ni, and P. Guo, "Indoor positioning method based on metameric white light sources and subpixels on a color image sensor," *IEEE Photon. J.*, vol. 8, no. 6, pp. 1–10, Dec. 2016.
[36] H. Maestre, A. J. Torregrosa, and J. Capmany, "IR image upconversion under dual-wavelength laser illumination," *IEEE Photon. J.*, vol. 8, no. 6, pp. 1–8, Dec. 2016.
[37] H. Hu, L. Zhao, B. Huang, X. Li, H. Wang, and T. Liu, "Enhancing visibility of polarimetric underwater image by transmittance correction," *IEEE Photon. J.*, vol. 9, no. 3, pp. 1–10, Jun. 2017.
[38] W. He *et al.*, "Adaptive depth imaging with single-photon detectors," *IEEE Photon. J.*, vol. 9, no. 2, pp. 1–12, Apr. 2017.